Strong positive allometry of bite force in leaf-cutter ants increases the range of cuttable plant tissues

Frederik Püffel *[1], Flavio Roces[2] & David Labonte †[1]

[1]Department of Bioengineering, Imperial College London, UK
[2]Department of Behavioural Physiology and Sociobiology, University of Würzburg, Würzburg, Germany

Atta leaf-cutter ants are the prime herbivore in the Neotropics: polymorphic foragers harvest plant material from the nest surroundings to grow a fungus as crop. Efficient foraging involves complex interactions between worker-polymorphism, task-preferences and plant-fungus-suitability; it is, however, ultimately constrained by the ability of differently-sized workers to generate forces large enough to cut vegetation. In order to quantify this ability, we measured bite forces of *A. vollenweideri* leaf-cutter ants spanning more than one order of magnitude in body mass. Maximum bite force scaled almost in direct proportion to mass; the largest workers generated peak bite forces 2.5 times higher than expected from isometry. This remarkable positive allometry can be explained via a biomechanical model that links bite forces with substantial size-specific changes in the morphology of the musculoskeletal bite apparatus. In addition to these morphological changes, we show that bite forces of smaller ants peak at larger mandibular opening angles, suggesting a size-dependent physiological adaptation, likely reflecting the need to cut leaves with a thickness that corresponds to a larger fraction of the maximum possible gape. Via direct comparison of maximum bite forces with leaf-mechanical properties, we demonstrate (i) that bite forces in leaf-cutter ants need to be exceptionally large compared to body mass to enable them to cut leaves; and (ii), that the positive allometry enables colonies to forage on a wider range of plant species without the need for extreme investment into larger workers. Our results thus provide strong quantitative arguments for the adaptive value of a positively allometric bite force.

Introduction

Leaf-cutter ants are remarkable in many ways: They are the world's first farmers; their colonies collect plant material to grow a fungus as crop – a mutualism that originated around 50 million years ago [1, 2]. They are considered the principal herbivore in the Neotropics; *Atta* ants are estimated to consume about 15 % of the foliar biomass produced by Neotropical trees [3, 4]. And last, they display a level of polymorphism, linked to size-dependent task-preferences and a complex ecology, exceptional even within social insects [e. g. 5, 6].

Among the diverse tasks arising in a leaf-cutter ant colony are brood care, fungus gardening, worker transport, soil excavation, nest defence and foraging [2, 5, 7]. In particular foraging behaviour has received considerable attention, as it is central to leaf-cutter ant ecology [e. g. 5, 8–34]. Key to foraging success is the cutting of small fragments from vegetation – the energetically most demanding task faced by the colony [35]. Although many aspects of foraging involve complex biological interactions [e. g. 36], cutting plant fragments is, to first order, a mechanical problem: The ability to cut a leaf or fruit is determined by the maximum available bite force, the morphology of the mandible, and the material and structural properties of the plant. Perhaps surprisingly, this mechanical foundation of leaf-cutting has received comparatively little quantitative attention [e. g. 37–39]. Larger workers may be reasonably expected to produce larger bite forces, and may thus be able to cut a wider range of plant materials. Indeed, they tend to be more likely to cut tougher and denser leaves [5, 8, 40–43]. Understanding the exact relation between bite force and worker size is crucial for the analysis of leaf-cutter ant foraging behaviour, because it holds the key to distinguish between foraging assignments based on ability (which ants can cut a given leaf) vs. suitability (which ants are best suited to cut a given leaf).

This distinction is relevant for assessing the evolution and possible adaptive advantage of worker polymorphism, and for predictions on 'optimal' foraging strategies based on ergonomic considerations [e. g. 8, 30, 43].

We previously predicted the scaling of bite force based on the morphology of the bite apparatus in *Atta vollenweideri* leaf-cutter ants [44]. However, direct experimental confirmation of this prediction is missing and difficult to obtain, because ants are small. To make matters worse, bite forces in insects generally depend on the mandibular opening angle [45–47], which is challenging to control experimentally. Here, we address both difficulties with the help of a custom-built bite force set-up and first principles biomechanical analysis. We report direct bite force measurements for ant workers spanning more than one order of magnitude in body mass, relate our results to the foraging behaviour of leaf-cutter ant colonies, and discuss both the magnitude and scaling of bite forces in a comparative framework.

Materials & methods

Study animals

Bite force experiments were conducted with *A. vollenweideri* ants from three colonies, all founded and collected in Uruguay in 2014 (see Fig. 1A). The colonies were kept at 25°C and 50 % humidity in a climate chamber under a light:dark cycle of 12 h:12 h, and were fed with fresh bramble leaves, cornflakes and honey water *ad libitum*. We collected around 80 workers from the foraging areas of each colony (n = 248), covering approximately the entire size range (1 - 50 mg). We excluded minims (body mass < 1 mg), because their bite apparatus is morphologically distinct, and they do not generally partake in foraging [44, N Imirzian, F Püffel and D Labonte, in preparation].

Experimental set-up

Bite forces were measured with a custom-built set-up based on a capacitive force sensor (SingleTact S8-1N, Pressure Profile Systems, Inc., California, USA, data acquisition frequency 33 Hz, maximum force 1 N, resolution 2 mN). In order to distribute the force equally across the sensor area, we used a lever mechanism to convert *point*-like bite forces into an *areal* compression (see Fig. 1B). Ants bit onto two thin bite plates (1 mm long, and $\approx$ 0.15 mm thick, see Fig. 1D), protruding from two mechanically uncoupled beams (6 x 6 x 40 mm and 6 x 12 x 6 mm, respectively). Both beams and the terminating bite plates were manufactured in one single piece from stainless steel to minimise compliance, using electrical discharge machining. The beam that transmits the bite force to the sensor was connected to a metal base plate, made from a single aluminium block using CNC milling, via a small hinge placed in the beam centre. As an ant bites onto the bite plates, the opposite end of this pivoting beam is pressed onto the sensor, which is glued to a vertical wall protruding from the base. At the maximum load of 1 N, the sensor only deforms approximately 10 μm [manufacturer data]. Because the gear ratio of the pivoting beam is unity, the magnitude of this deformation is equivalent to the maximum displacement of the bite plate arising from beam rotation. As bite plate bending is also negligible (see SI), we measured approximately isometric bite forces. The second beam, in turn, was connected to a lubricated rail, so that its position relative to the pivoting beam can be altered via a stepper motor (28BYJ-48, 5 V), connected to a gearing system 3D printed from PLA. This design allowed us to vary the distance between the two bite plates by less than 100 μm per motor step. The minimum required gape to bite both bite plates, equivalent to the shortest distance between their outer surfaces, was 0.5 mm, and the largest gape used during experiments was 3.0 mm. This range is similar to the range of head widths of the ants used in this experiment (1.1 - 4.5 mm).

In order to extract coordinates of key landmarks (see below), a top-down camera was synchronised to the sensor recording, and recorded the bite experiments at 30 fps, (camera module v 2.1, 8 MP, Raspberry Pi Foundation, Cambridge, UK; with a Black Eye HD macro lens, Eye Caramba Ltd., Helsinki, Finland). A mirror, tilted 45° with respect to the camera plane, provided depth information. Force sensor, motor, camera and a touchscreen (7 inch HDMI-LCD Display, Elecrow, Shenzhen, China) were connected to a Raspberry Pi (v 3B+, Raspberry Pi Foundation, Cambridge, UK). The system was operated via a custom software written in Python [v 3.5, see 48, and SI for details on the user interface and circuit].

Sensor calibration, accuracy and precision

The sensor was calibrated using a series of calibration weights (Kern & Sohn GmbH, Balingen, Germany), suspended from the pivoting lever via a thin cotton thread (the weight of the cotton thread was small, $\approx$ 0.015 g , and hence neglected). The thread was placed at around one-quarter of the length of the bite plate measured from its base, resulting in a moment arm around the pivot of $|\mathbf{L}_{p,cal}| \approx 20.25$ mm. The set-up was rotated such that the measurable force vector aligned with gravity (see Fig. 1E). We used 20 weights between 5 and 100 g; a weight of 1.4 g was required to establish equilibrium around the pivot, and was consequently subtracted from all readings. The range of effective weight forces was hence 35 - 970 mN, approximately spanning the range of measured bite forces. Each weight was suspended five times in random order, and the steady-state sensor reading averaged across $\approx$ 2 s was used for sensor calibration. The relationship between weight and sensor output was characterised via an Ordinary Least Squares regression on $\log_{10}$-transformed data in order to prioritise minimisation of relative error over absolute error; the high R-squared of the regression line indicates robust calibration (R^2 = 0.993, see Fig. 1E).

To quantify calibration accuracy and precision, five additional weights (7 - 87 g) were measured three times each, and the relative error was calculated as $\varepsilon = 1 - |\mathbf{F}_w|/|\mathbf{F}_x|$, where $\mathbf{F}_x$ is the predicted and $\mathbf{F}_w$ is the measured force, respectively (see Fig. 1F). The average measurement error, the sensor accuracy, was 2 ± 6 % independent of weight [Linear Mixed Model (LMM) with weight as fixed and repetition as random effect: $\chi^2_1 = 0.38$, p = 0.53; the average magnitude of the measurement error was 5 ± 4 %]; the standard deviation indicates the precision of the measurements.

To quantify sensor noise, the output of the unloaded sensor was recorded for 100 s. Discrete Fourier transformation suggested a constant power spectral density, indicating white noise [49, p. 61] This noise had a standard deviation of 1 mN and a range of -5 to 4 mN. The maximum positive value of this range was about eight times smaller than the smallest measured bite force (see Fig. 1C). Sensor drift was significant [Spearman's correlation coefficient: $r_{s,2867}$ = -0.26, p < 0.001; see manufacture data sheet], but small enough to be inconsequential across the time scale of our measurements (cf. 1 mN/min vs $\approx$30 - 60 s).

In a last validation step, we directly compared measurements with our set-up with those of an established set-up based on a substantially more expensive piezoelectric sensor [50, 51]. To this end, maximum bite forces of three house crickets (*Acheta domesticus*) were measured with three repetitions on both set-ups, by two independent operators each. A LMM with set-up and operator as fixed and specimen as random effect showed no significant influence of neither set-up nor operator on bite forces [LMM versus random intercept model: $\chi^2_2 = 3.83$, p = 0.15; set-up: t_{31} = 1.68, p = 0.10; operator: t_{31} = 0.95, p = 0.35].

The camera was calibrated assuming an inverse size-distance relationship, $L_2 S_2 = L_1 S_1$, where S_1 and S_2 are the apparent sizes of an object at distances L_1 and L_2 to the camera aperture. The apparent size of a calibration target (5 units on 1 mm-grid paper), placed on the top surface of the metal base at a distance $L_1 \approx 32$ mm to the camera, was measured from ten images, and the pixel-to-mm conversion factor C_1 was extracted. This conversion factor changes approximately in direct proportion to the camera distance as $C_2 = C_1 L_2 / L_1$, where L_2 is the distance between the camera and the imaged object. In contrast to L_1, L_2 is not constant, but varies with the vertical position of the object coordinate, which was extracted using the mirrored side view.

For validation, the grid paper was photographed at 25 different positions along the bite plate, extracted from five trials, and its physical size was calculated from the calibration. The relative error was 1 ± 2 %. This error changed significantly with grid paper-lens distance – the physical dimensions were increasingly underestimated at smaller distances [LMM with lens distance as fixed effect and trial as random effect: $\chi^2_1 = 6.94$, p < 0.01]. This effect, however, was miniscule (1.5 % across the entire bite plate length, 6 mm), corresponding to only $\approx 60\,\mu$m, or about 10 % of the smallest measured mandible length; it is thus considered negligible.

Experimental protocol

To measure bite forces, individual ants were held in front of the bite plates using insect tweezers. Ants were pleasantly eager to bite, typically executing numerous bite cycles in quick succession (see Fig. 1C). After completing at least five bite cycles, or exceeding a total bite duration of 10 s, the measurement was terminated, each ant was weighed (AX304 Microbalance, 310 g x 0.1 mg, Mettler Toledo, Greifensee, Switzerland) and isolated, and the maximum force was extracted. To obtain bite forces from a maximum range of sizes and varying opening angles without pseudoreplication, we measured each ant only once at a single bite plate distance. In practice, we gradually increased the bite plate distance from 0.5 to 3.0 mm; for each distance, we used ants of all sizes capable of biting onto the plates. For small plate distances, this included almost all ants; for the largest plate distance, however, only larger specimen were able to bite. We assume that ants bit with maximum muscle activation at all opening angles, as indicated by measurements involving direct muscle stimulation in closely related *Atta cephalotes* [47].

Extraction of landmarks

In order to obtain the opening angle, the orientation of the bite force vector, and the length of the mandible outlever (see below), we extracted the coordinates of a series of landmarks from the video frame corresponding to the time of maximum bite: (i) the contact point between mandible and bite plate; (ii) the tip of the most distal and proximal mandibular teeth; (iii) the mandible joint centre (defined as in [44]); and (iv) a pair of distinct head spikes (see Fig. 1D). In addition, we extracted the orientation of the mandible joint axis $\hat{\mathbf{R}}$ via kinematics analysis of the mandible motion [47, V Kang, F Püffel and D Labonte, in preparation]. In order to position $\hat{\mathbf{R}}$ on the biting ant, we introduced a local head coordinate system ($\mathbf{e}_1$, $\mathbf{e}_2$, $\mathbf{e}_3$) based on the vectors connecting the joint centre with the tips of both head spikes, $\mathbf{S}_l$ and $\mathbf{S}_r$, respectively. The coordinate axes were defined as $\mathbf{e}_1 = \mathbf{S}_l/|\mathbf{S}_l|$, $\mathbf{e}_3 = (\mathbf{S}_l \times \mathbf{S}_r)/|\mathbf{S}_l \times \mathbf{S}_r|$, and $\mathbf{e}_2 = \mathbf{e}_3 \times \mathbf{e}_1$. The estimated rotational axis was then projected onto this local head coordinate system (for more details, see SI). In line with previous work [52], we define the opening angle as the angle between the lateral head axis and the largest effective outlever $\mathbf{L}_{o,eff,d}$. The lateral head axis was defined as the vector connecting both head spikes (see Fig. 1D).

Confounding effects due to size-differences

Measuring bite forces across a large size range poses at least two challenges. First, the signal-to-noise ratio typically decreases with animal size, as smaller animals generally bite with less force. We addressed this challenge by selecting a force sensor capable of measuring small and large bite forces with sufficiently high resolution (see above). Second, the characteristic dimensions of the set-up are relatively larger for small animals. The implications of this size-effect are perhaps less obvious and, unfortunately, more complex. To appreciate the problem, consider a small ant of 3 mg body mass biting onto bite plates that are 1 mm apart. This bite plate distance is approximately equal to the distance between both mandible joints; a bite with the distal-most teeth would thus involve a mandibular opening angle of about 90°. For a bite with the most proximal teeth, in turn, the opening angle is larger, around 110° (see Fig. 1A), and the effective outlever is smaller. Consider next a large ant of 45 mg biting onto the same bite plates. For a distal bite, the bite plate distance corresponds to only 40 % of the joint distance, and thus a much lower opening angle of about 70°. Notably, the ant's ability to bite proximally is limited because the length of the mandible blade exceeds the length of the bite plate by about 20 % (see Fig. 1D). Evidently, for a given configuration of the experimental setup, both the range of possible mandibular opening angles and bite positions along the mandible blade vary systematically with size. Because both directly affect the magnitude of bite force [see Eq. 2 and 47], an unbiased comparison of bite force magnitude across animal sizes, requires four corrective steps, implemented here with the ultimate aim to extract the maximum bite force an ant worker can produce when biting with an equivalent point of her mandible (see Fig. 2). First, we correct for the misalignment between *measurable* force vector and *applied* bite force vector. Second, we correct for differences in moment arms around the lever pivot, arising from variation of the bite contact point. Third, we account for variation in bite position along the mandible blade, which alters the mechanical advantage of the force transmission system. Fourth, we account for differences in mandibular opening angle during exertion of the maximum bite force.

The first correction is necessary, because the sensor measures 1D compression, $\mathbf{F}_{b,m}$, but the applied bite force vector, $\mathbf{F}_b$, may deviate from this line of action by a misalignment angle α (see Fig. 1D). The orientation of $\mathbf{F}_{b,m}$ is approximately equal to the plane normal of the bite plate; the orientation of the bite force vector is defined by the cross product between mandible outlever $\mathbf{L}_{o,c}$ and the rotational axis, where $\mathbf{L}_{o,c}$ is the vector connecting joint centre and the bite contact point [for more details, see 47]. This correction was typically larger for larger animals, which more frequently bit at opening angles below 90° (see results), leading to larger misalignment angles.

The second correction is necessary, because the point of force application on the bite plate itself may vary across ants – smaller ants have shorter mandibles and are thus more likely to bite at the distal part of the bite plates, so changing the lever arm around the pivot, $\mathbf{L}_p$. To account for variation in lever arm, we introduce the correction term $\Gamma = |\mathbf{L}_{p,cal}|/|\mathbf{L}_p|$. Γ was always close to 1, as the length of the bite plate is small in comparison to the total length of the lever arm ($\approx 5\,\%$); the effect of this correction was thus miniscule.

The third correction is necessary, because the bite force may be transferred onto the bite plate at an arbitrary position along the mandible; an ant biting with the distal end of its mandible may use the same muscle effort but nevertheless produce a smaller measured bite force than an ant biting with the proximal end of its mandible, because the mechanical advantage of the force transmission system differs [see e. g. 53]. To correct for this variation, we converted the measured bite force into an equivalent bite force at a fixed point on the mandible blade (the most distal tooth tip). To this end, two effective mandible outlevers, each defined as the projection of the outlever onto the plane of rotation, were calculated for the contact point and the most distal tooth tip, respectively, as $\mathbf{L}_{o,eff} = \mathbf{L}_o - (\hat{\mathbf{R}} \cdot \mathbf{L}_o)\hat{\mathbf{R}}$ [for more details, see 47].

After implementation of corrections (i-iii), the magnitude of the bite force $|\mathbf{F}_b|$ follows as:

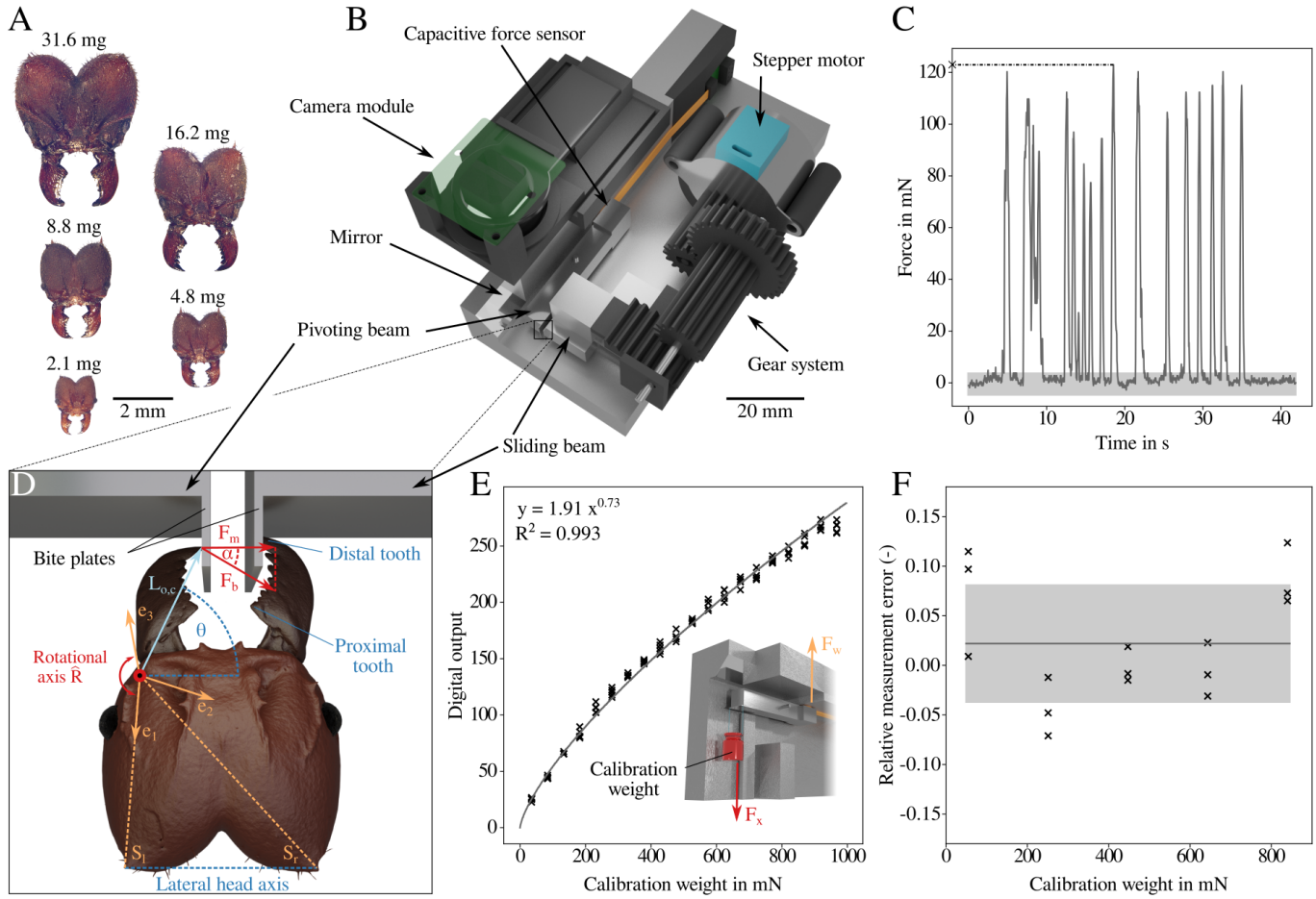

Figure 1 | (**A**) We measured bite forces of polymorphic *Atta vollenweideri* leaf-cutter ants ranging between 1.5 and 46.8 mg in body mass. (**B**) To measure bite forces, we built a custom-designed force setup based on a capacitive force sensor and a lever mechanism. The ants bit onto two bite plates, one protruding from a pivoting beam connected to the force sensor, the other protruding from a sliding beam. The distance between the two bite plates can be varied by moving the sliding beam via a geared stepper motor. Bite experiments were filmed with a top-down camera, which also recorded a side view from a 45° mirror. (**C**) When placed in front of the bite plates, ants readily bit. The measured forces exceeded the sensor noise (shaded area) by at least a factor of eight. From each force trace, the maximum force (cross) was extracted for further analysis. (**D**) From the video recordings, we further extracted the coordinates of the mandible joint centre, head spikes $\mathbf{S}_l$ and $\mathbf{S}_r$, outlever length $\mathbf{L}_{o,c}$, and the most distal and proximal tooth tips. The rotational axis of the mandible $\hat{R}$ was projected onto the local head coordinate system ($\mathbf{e}_1$, $\mathbf{e}_2$, $\mathbf{e}_3$). The mandibular opening angle θ was defined as the angle between the lateral head axis, span by the head spikes, and the projection of the largest outlever onto the plane of rotation. The magnitude of the bite force $|\mathbf{F}_b|$ was extracted from the measured force $\mathbf{F}_{b,m}$ and the misalignment angle α, measured from the video recordings, as defined by Eq. 1. (**E**) For sensor calibration, we suspended weights between 5 and 100 g from the bite plate of the pivoting lever. A linear regression on $\log_{10}$-transformed data characterised the relationship between measured output and force with high accuracy ($R^2 = 0.993$). (**F**) A subsequent error analysis using intermediate weights between 7 - 87 g yielded relative errors between measured and expected forces of 2 % (accuracy, black line) with a standard deviation of 6 % (precision, shaded area), independent of weight (see text).

$$|\mathbf{F}_b| = \Gamma \frac{|\mathbf{F}_{b,m}|}{\cos\alpha} \frac{|\mathbf{L}_{o,eff,c}|}{|\mathbf{L}_{o,eff,d}|} \tag{1}$$

$$|\mathbf{F}_b|(\theta) = \sigma(\theta) A_{phys} \cos[\phi(\theta)] \frac{|\mathbf{L}_{i,eff}(\theta)|}{|\mathbf{L}_{o,eff,d}|} \tag{2}$$

The fourth and last correction is necessary, because changes in opening angle are associated with changes in both muscle length and mechanical advantage. The resulting variation in bite force magnitude can be substantial; in *A. cephalotes* majors, bite forces at small opening angles are around five times larger than those at large opening angles [see 47, and Fig. 2].

In order to implement this correction, we first recognise that bite force is a function of both morphological and physiological parameters; it is determined by muscle stress σ, the physiological cross-sectional area of the mandible closer muscle A_{phys}, the average fibre pennation angle ϕ, and the mechanical advantage of the mandible lever system, defined as the ratio between effective in- and outlever $|\mathbf{L}_{i,eff}|/|\mathbf{L}_{o,eff,d}|$ [see 44, 47, for details]:

We analysed 13 tomographic scans of *A. vollenweideri* leaf-cutter ants across the size range but excluding minims in order to extract muscle volume, average muscle fibre length, pennation angle, and the effective mandible levers [for details, see 44]. Fibre length, pennation angle and effective inlever are functions of the mandibular opening angle. We previously demonstrated that these functions can be accurately predicted from first principles, using a small set of assumptions, geometry and reference measurements at a single opening angle [47]. For this study, we assume that all fibres of the closer muscle attach to the tendon-like apodeme via thin filaments [which holds for 98 % of fibres in *A. vollenweideri*, 44]; the length of these filaments determines the change of fibre length with opening angle, and was extracted

from the scans (for more details, see SI). We define the physiological cross-sectional area as the muscle volume divided by the optimal fibre length at which the muscle stress is maximum, L_{opt} [47]. Muscle fibres which are stretched or shorten deviate from this optimum length, and as a result the muscle stress decreases due to characteristic force-length effects [54–56]. The magnitude of the decrease may be characterised by an empirical shape parameter β via $\sigma(\theta) = \sigma_{max} e^{-\beta(1-L_f(\theta)/L_{opt})^2}$ [47]. The maximum muscle stress $\sigma_{max} = 1.16\,\text{MPa}$ and $\beta = 5.34$ were taken from Püffel et al. [47], where they were determined experimentally for closely related *A. cephalotes* majors. We make the simplifying assumption that these parameters are size-independent, and this assumption is supported by the resulting agreement between theoretical prediction and measured bite force (see below).

The mandibular opening angle at which the muscle stress is maximum, $L_f(\theta_{opt}) = L_{opt}$, was then estimated via a non-linear least squares numerical fitting routine of Eq. 2 in python [v 3.9 48]. Notably, θ_{opt} may be reasonably expected to vary with body size, as it is sensitive to head capsule geometry which changes with size in *A. vollenweideri* [see 44, and N Imirzian, F Püffel and D Labonte, in preparation]. In order to investigate the size-dependence of θ_{opt}, we selected bite force measurements from individuals with a body mass that differed by no more than $\approx 25\,\%$ from the individuals for which we obtained morphological data from μCT scans. Each size-class bin contained at least eight bite force measurements, except for the largest and smallest ant, which contained two and three bites, respectively.

In order to implement the opening angle correction across worker sizes, we first characterised the size-dependent relationship between bite force and opening angle as outlined above. Next, we calculated a database containing the relationship between predicted bite force, normalised with its maximum, $\hat{\mathbf{F}}$, opening angle and size. We rescaled the measured forces, corrected via Eq. 1, to the force expected at an *equivalent* mandibular opening angle; the angle θ_{max} at which bite forces are maximal, $|\mathbf{F}_{b,max}| = |\mathbf{F}_{b,\theta}|/|\hat{\mathbf{F}}_{\theta}|$. The magnitude of this correction thus depends on both the size and the mandibular opening angle of the biting ant; the corrected value used for the final analysis is the maximum force the animal can transmit at the distal mandibular tooth (see Fig. 1D).

Data curation and statistical analysis

We pooled bite force data from all three colonies, because the relationship between bite force and body mass was independent of colony both before and after correcting for differences in opening angle [Analysis of covariance (ANCOVA) on $\log_{10}$-transformed data, before correction: $F_{2,242} = 1.26$, $p = 0.28$; after correction: $_{2,242} = 0.85$, $p = 0.43$]. Out of 248 bite force measurements, three slightly exceeded the range of calibration forces; two were lower and one higher, but all within 15 % to the nearest calibration force. These measurements neither appeared to be outliers, nor altered the scaling relationship (see results), and were hence kept for the analysis. Scaling relationships were characterised with Ordinary Least Squares (OLS) and Reduced Major Axis (RMA) regression models on $\log_{10}$-transformed data in R [v 4.1, 57]. For simplicity, we only report the results of the OLS regressions in the text; the RMA regression results are provided in the SI. Scaling coefficients tend to be higher for RMA regressions [also see 58]; however, the main conclusions of this study are supported by both.

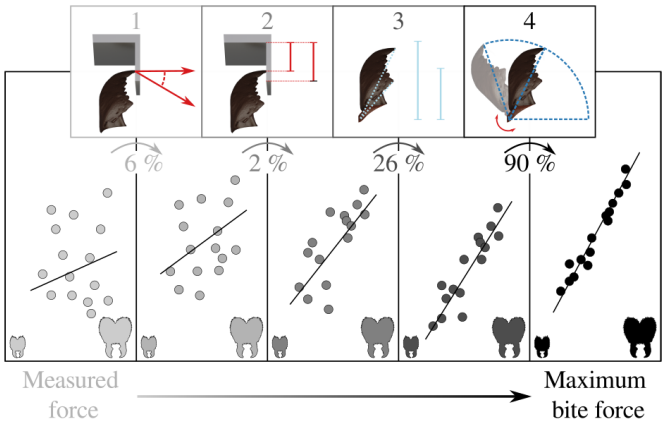

Figure 2 | In order to extract the maximum bite force from the measured data, we account for four confounding effects: First, we account for the misalignment between bite force orientation and the force-sensitive axis. Second, we account for variation in bite contact point on the bite plate, which results in different moment arms. Third, we account for differences in bite position along the mandible blade, which determines the mechanical advantage of the musculoskeletal force transmission system. Fourth, we account for variation in mandibular opening angle, which is associated with variation in mechanical advantage, fibre length and pennation angle, all of which influence bite forces. Implementation of these corrections reduces the size-dependent variation introduced by the experimental design and animal behaviour, and thus enables an unbiased comparison of maximum bite force capacity across animals of different sizes. The data depicted in this schematic is not 'real' data, but merely serves for illustration. The 'actual' relative change in force caused by each correction, averaged for all ants, is shown in percent.

Results

Leaf-cutter ant bite forces increase with strong positive allometry

We measured bite forces of *A. vollenweideri* leaf-cutter ants spanning more than one order of magnitude in body mass, m. Measured bite forces $|\mathbf{F}_{b,m}|$ ranged from a minimum of 31 mN to a maximum of 1029 mN, and were proportional to $m^{0.79}$ [OLS 95 % CI: (0.74 | 0.85), $R^2 = 0.75$], suggesting positive allometry (isometry predicts $m^{0.67}$). After correcting for force orientation, and bite position along the bite plate and mandible blade, respectively, bite forces, $|\mathbf{F}_{b,\theta}|$, ranged between 19 and 901 mN (see Fig. 2 and Eq. 1), and were proportional to $m^{0.85}$ [OLS 95 % CI: (0.79 | 0.92), $R^2 = 0.74$], in substantial excess of the scaling coefficient of $|\mathbf{F}_{b,m}|$ (see Fig. 3B). However, this scaling relationship is still influenced by systematic differences in mandibular opening angle, which, as expected, were systematically smaller for larger animals [Analysis of variance (ANOVA) on $\log_{10}$-transformed data: $F_{1,246} = 15.24$, $p < 0.001$].

In order to correct for the systematic differences in opening angle, we first assessed the size-dependence of the opening angle, θ_{opt}, at which muscle stress is maximum [see methods and 47]. Notably, θ_{opt} decreased significantly with body mass [OLS: slope = -0.09, 95 % CI: (-0.15 | -0.04), $p < 0.01$, $R^2 = 0.56$]: $\theta_{opt} \approx 70^\circ$ for a 1.5 mg ant, but $\theta_{opt} \approx 50^\circ$ for a 45 mg ant. Next, we calculated the opening angle at which the bite

force is maximum, θ_{max}. θ_{max} may differ from θ_{opt}, because bites with larger or smaller opening angles may involve a higher mechanical advantage, so counteracting any loss of force associated with isometric contractions at non-optimal fibre length [47]. θ_{max} decreased significantly with size [OLS: slope = -0.06, 95 % CI: (-0.10 | -0.03), $p < 0.01$, $R^2 = 0.59$, represented by the crosses in Fig. 3A]; the bite forces of a 1.5 mg and 45 mg ant are maximal at around 65° and 50°, respectively. Thus, the difference between θ_{max} and θ_{opt} is small, supporting our earlier conclusion that the musculoskeletal bite apparatus of leaf-cutter ants has a morphology which maximises the magnitude of the peak bite force [see 47].

Equivalent bite forces at θ_{max} and the most distal bite point scale with an even stronger positive allometry, $|\mathbf{F}_{b,max}| \propto m^{0.90}$ [OLS 95 % CI: (0.86 | 0.95), $R^2 = 0.86$]. The increase in scaling coefficient is surprising, because larger ants bit at significantly smaller opening angles; the intuitive expectation is thus that the bite forces of small ants were underestimated, and the scaling coefficient overestimated. However, this argument neglects the significant decrease of θ_{max}, which reverts the effect: because θ_{max} decreases more quickly than the opening angle increases, larger ants were measured at less favourable opening angles, and the scaling coefficient was underestimated.

Together, the four corrections result in a significant increase of the scaling coefficient by 0.11, or about 15 % [LMM with correction as fixed and sample number as random effect: $\chi^2_1 = 118$, $p < 0.001$], and in an increase of the R^2 from 0.75 to 0.86. The difference in scaling coefficient may appear small, but this impression is misleading: the difference in maximum bite force between ants varying in body mass by a factor of 30 is $30^{0.90} \approx 22$ compared to $30^{0.79} \approx 15$ – a drop by about 30 %. Clearly, a careful analysis of bite force measurements is required in order to draw meaningful conclusions on scaling relationships.

Discussion

Leaf-cutter ants are an ecologically and economically important herbivore [4, 6], foraging on a wide variety of plants with different mechanical properties [40, 41]. Key to foraging success is the ability of workers to produce bite forces sufficiently large to cut plant tissues [59]. How does this ability vary with worker size? In order to address this question, we measured the maximum bite forces of *A. vollenweideri* leaf-cutter ants spanning more than one order of magnitude in body mass. In the following discussion, we (i) connect the bite force allometry with its morphological and physiological determinants; (ii) discuss the magnitude and scaling of maximum bite forces in the context of foraging ecology; and (iii) place our findings in an evolutionary and comparative context.

Bite force allometry can be accurately predicted from muscle architecture and head morphology

Maximum bite forces of *A. vollenweideri* workers show strong positive allometry, $|\mathbf{F}_{b,max}| \propto m^{0.90}$. Due to the large variation in worker size, the effect of this positive allometry is rather extreme: the largest ant workers generate maximum bite forces about 2.5 times higher than a theoretical isometric worker with the same body mass, $(45/1)^{0.90-0.67} \approx 2.5$. Can this extreme positive allometry be understood from the morphology and physiology of the *Atta* bite apparatus?

We have previously extracted the relevant morphological bite force determinants in *A. Vollenweideri* workers from tomographic scans [see 44]. On the basis of these data, we predicted that bite force should scale as $m^{0.88}$, a positive allometry largely driven by a disproportional increase in physiological cross-sectional area of the mandible closer muscle [44]. This prediction is in rather close agreement with our bite force measurements. The small difference stems from the fact that we previously extracted the morphological bite force determinants from scans, where the mandibles were maximally closed, whereas θ_{max} varies across sizes (see Fig. 3A). In order to account for this variation in our morphological prediction, and to estimate the intercept of the scaling relationship, we use the stress and force-length shape parameter measured for closely related *A. cephalotes* [47], the change in θ_{opt} as observed in this work, and a biomechanical model which links morphology, opening angle and bite force to directly predict maximum bite forces [see 47, and Fig. 3A].

This calculation predicts a scaling of $m^{0.91}$ [OLS 95 % CI: (0.82 | 1.01), $R^2 = 0.98$], and an intercept of 1.42 [units: mN, mg; OLS 95 % CI: (1.32 | 1.52]. Both estimates are almost identical to the results obtained from direct measurements: $m^{0.90}$ (scaling coefficient), 1.46 (intercept) [units: mN, mg; OLS 95 % CI: (1.41 | 1.51)]. In other words, the ratio between maximum measured and predicted bite forces is close to unity (1.11±0.30), and independent of body mass [ANOVA on $\log_{10}$-transformed data: $F_{1,246} = 0.23$, $p = 0.63$, see Fig. 3D]. We thus conclude that the scaling of bite forces can be predicted to reasonable accuracy from morphological measurements.

Predicting bite performance from morphology is of considerable interest to evolutionary biologists, palaeontologists and biomechanists alike, as *in-vivo* force measurements are often challenging if not impossible to obtain. Consequently, theoretical models to predict maximum bite force have been developed and deployed for numerous taxa [e. g. 47, 60–63]. In arthropods, the two key obstacles facing such theoretical efforts are the extraordinary variation in reported muscle stresses [e. g. 64, 65], and the uncertainty in estimates of the physiological cross-sectional area, which requires knowledge of the optimal fibre length [47]. The fact that we were able to accurately predict both the magnitude and scaling of bite forces in *A. vollenweideri* using physiological parameters measured in closely related *A. cephalotes* suggests that muscle stress and shape parameter β are conserved across sizes and within *Atta*, cautiously indicating that the intraspecific and intrageneric variation of bite forces may be predictable based on morphological data alone.

Positive allometry of bite force has substantial benefits at colony level

Bite force are a non-pareil performance measure which influences access to food sources and high-quality mating partners [66]. As a result, the variation in morphology and physiology of the bite apparatus across species often reflects species-specific needs [45, 67–70]. What needs have shaped the evolution of bite performance in *Atta*?

Atta ants are known for their 'catholicity of taste' [71, 72]; a single colony may forage on more than 100 plant species at once, spanning a large range of chemical and mechanical properties [40, 73]. Foraging is not completely indiscriminate, however: for example, foragers seem to prefer young (tender) over

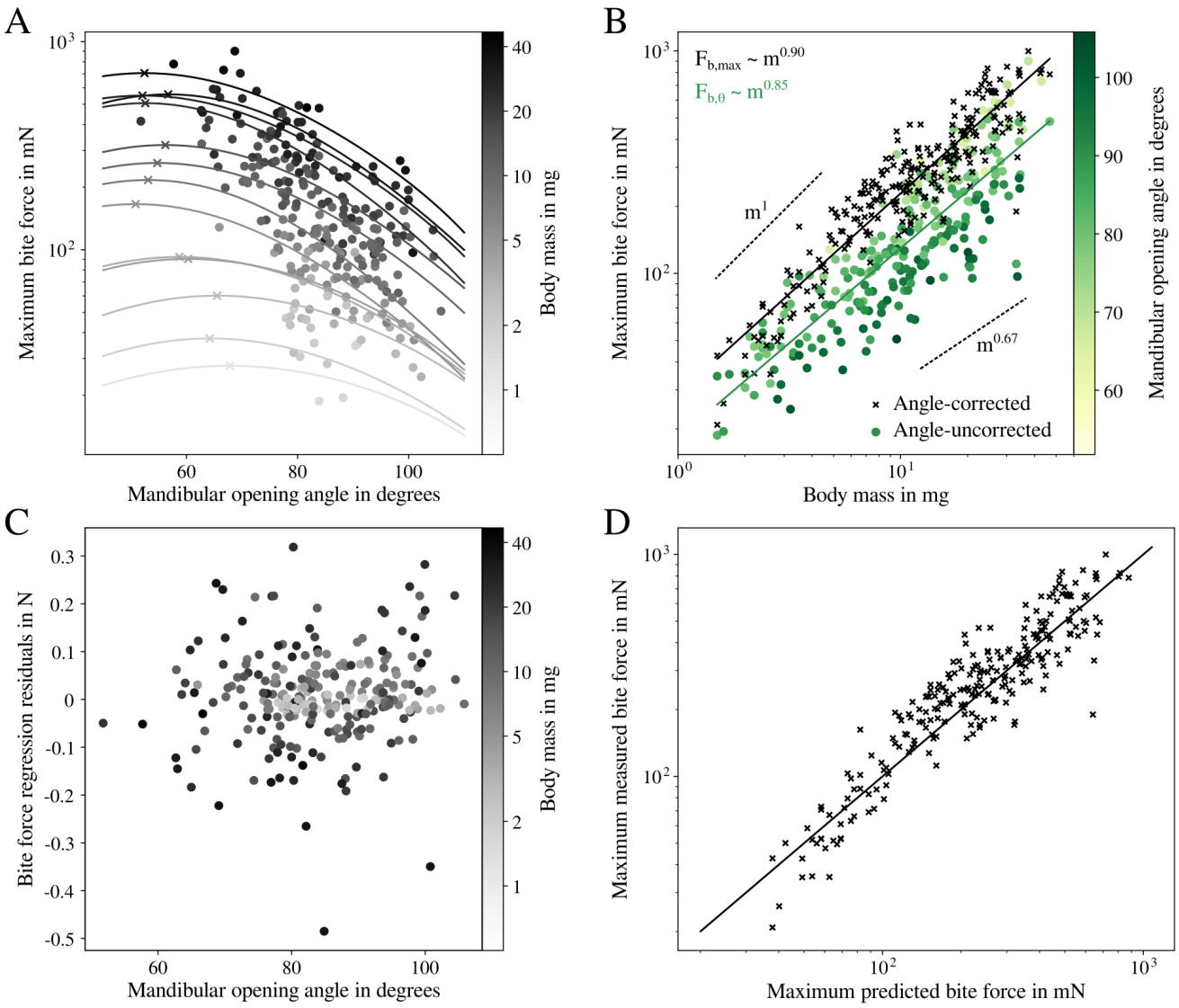

Figure 3 | (**A**) Maximum bite force is determined by the morphology of the bite apparatus and the physiology of the mandible closer muscle. The morphological force determinants were extracted from 13 tomographic scans of *Atta vollenweideri* scans across all sizes excluding minims. The physiological determinants were determined experimentally for closely related *Atta cephalotes* majors [47], except for the mandibular opening angle at which the muscle stress is maximum. This 'optimum' angle was fitted numerically using bite forces measured for ants similar in size to those for which tomographic scans were available (circles). The solid lines represent the predicted bites forces from morphology and physiology across mandibular opening angles, calculated via a first-principle biomechanical model derived in [47]. The maxima of these predictions (crosses) shift to significantly larger opening angles for smaller ants [Ordinary Least Squares (OLS) regression: slope = -0.09, $p < 0.01$]. (**B**) Bite forces, corrected to an equivalent mandibular opening angle and bite points on the mandible (crosses), scale with strong positive allometry [$\text{mass}^{0.90}$, OLS 95 % CI: (0.86 | 0.95), $R^2 = 0.86$], far surpassing the parsimonious prediction from isometry ($\text{mass}^{0.67}$); bite forces are almost directly proportional to body mass. The scaling coefficient exceeds the estimate from angle-uncorrected data [$\text{mass}^{0.85}$, OLS 95 % CI: (0.79 | 0.92), $R^2 = 0.74$], represented by the green line and circles. (**C**) The residuals of the regression on corrected maximum bite forces are independent of mandibular opening angle [ANOVA: $F_{1,246} = 2.43$, $p = 0.12$], supporting the validity of the angle-correction. (**D**) The corrected measured bite forces are in excellent agreement with a quantitative prediction from morphology and physiology, as demonstrated by the identity function (solid line). The predicted forces are the result of an OLS regression on $\log_{10}$-transformed data between force maxima (crosses in figure part A) and body mass of the scanned ants. We note that predicted and corrected forces are not strictly independent; the optimum opening angle, affecting the force prediction, was fitted using the measured bite forces, and the correction factor, applied to the measured forces, was determined via the normalised predictions.

old (tough) leaves from the same plant [40, 42, 73, 74]. Notably, this preference disappears when pre-cut leaf fragments are offered instead [41, 42], suggesting that foraging decisions are not solely driven by plant chemistry, but also by mechanical considerations. Because larger ants typically cut tougher and denser leaves than smaller ants [5, 8, 16, 17, 40, 41], we surmise that these mechanical considerations are further confounded by size. From these simple observations emerge two key demands on bite forces in *Atta*: its magnitude must be large enough to cut a representative leaf, and its scaling determines the range of plant leaves that can be cut by workers of different size.

In order to contextualise the magnitude of the bite force, we estimate the forces required to cut leaves. Consider a blade-like tool which exerts a force of magnitude F to make a cut of length dx through a thin sheet of thickness t. The work done, $\int F dx$, supplies the energy required to create the new surface arising from the cut, $Gtdx$, where G is the energy associated with a unit area of surface; the cutting force then follows as $F_c \approx Gh$.

This calculation provides a lower bound on the required force, because it neglects the influence of friction, tool geometry and sheet bending [e. g. 75–77]. Onoda et al. used cutting tests to quantify a proxy for G, the work per unit fracture length to cut leaf lamina of known thickness, for about 1000 tropical plant species [78, 79, we note that although *A. vollenweideri* is often referred to as a grass-cutting ant, workers also cut dicotyledonous leaves, also see 80]. On the basis of the simple mechanical model and these extensive experimental results, we estimate that the forces required to cut tropical leaves vary between 7 - 828 mN. The median required cutting force of 82 mN can be generated by a worker of about 5 mg (see Fig. 4), and we submit that this finding strongly suggests that the remarkable magnitude of bite forces in *A. vollenweideri* (see below) arises from the ecological need to cut leaves.

In order to contextualise the positive allometry of bite force, we next calculate the fraction of cuttable leaves as a function of worker size, both for allometric and hypothetically isometric workers (see Fig. 4). A direct comparison between two populations of workers which follow different scaling laws requires to specify the body mass at which the two scaling lines intersect. Do large workers bite relatively more strongly, or small workers relatively more weakly? This question cannot be answered *a priori*, and we thus refer to three biological arguments instead: First, the worker-size distribution in leaf-cutter ant colonies typically has a long right tail, i. e. the vast majority of foraging workers is relatively small [5, 10, 81, 82]. Second, large workers are only produced in larger numbers once colonies exceed a critical size [10, 82]. Third, larger workers are more 'costly' than smaller workers. On the basis of these arguments, increasing the bite force capacity disproportionally may represent a strategy to minimise the cost associated with a unit increase in maximum bite force. A disproportionate decrease of bite forces, in contrast, appears to have no obvious biological benefit. Thus, small workers may represent a reasonable generalist 'starting point', and we choose a weight of 1 mg, at the transition between minims and medias [5, 44], as intersection mass.

Viewed in this light, the positive allometry of bite force has substantial benefits for the colony for at least two reasons. First, the maximum bite force of an allometric worker with a body mass of 27 mg, at the upper end of forager sizes typically reported in *Atta* [12, 16, 17, 29, 83], exceeds that of an equally-sized isometric worker by a factor of two (see Fig. 4A). Provided that the data reported by Onoda et al. [79] are representative, this difference increases the fraction of cuttable leaves from 94 % to almost 100 % (see Fig. 4B). This difference may seem small, but this perception is erroneous: A large isometric forager would need to be three times heavier to cut the same fraction of leaves. Second, the smallest worker that can cut the median leaf almost halves in mass between isometric and allometric workers (5 to 3 mg, see Fig. 4B). As the majority of workers are typically small [82], the positive allometry thus significantly increases the fraction of the colony that can partake in leaf-cutting: an allometric forager of 5 mg can cut up to 70 % of leaves, a whopping 20 % more than its isometric counterpart. This substantial increase in the size range which can forage on a large number of plant species facilitates flexible task assignment, likely increases harvesting speed and overall influx of nutrients to the nest, and may thus be reasonably expected to enhance colony fitness.

In addition to the positive allometry of maximum bite force, our results revealed a significant decrease in opening angle at which fibres take their optimum length, θ_{opt}. We note that the last correction step, which led to this conclusion, is complex. In contrast to the first three corrections steps which are based on geometrical relations and thus have high predictive accuracy, it involves assumptions on muscle physiology, and neglects passive force-length effects due to muscle or connective tissue elasticity [47]. In support of the validity of our angle correction and the resulting conclusion, three independent lines of evidence may be offered. First, the angle-corrected regression analysis explains a substantially larger share of the variation of bite force with mass (86 % vs 74 % for $|\mathbf{F}_{b,\theta}|$, see Fig. 3B). Second, the regression residuals are independent of opening angle [ANOVA: $F_{1,246} = 2.43$, $p = 0.12$, see Fig. 3C], which does not hold without angle-correction [ANOVA: $F_{1,246} = 148$, $p < 0.001$]. Third, the relationship between θ_{opt} and body mass remains significant even after removing the smallest and largest size classes, which contain fewer data points (see methods), and are thus associated with higher uncertainty [OLS: slope = -0.08, 95 % CI: (-0.15 | -0.01), $p < 0.05$, $R^2 = 0.44$]. Our result therefore appears statistically robust, and we next offer a cautious functional interpretation. Ant workers large or small may often forage on the same plant leaf. Although their size differs, the characteristic dimension of the leaf lamina – its thickness – is the same. Because cuts are typically initiated at the leaf-edge by drawing mandibles together like scissors, ants need to produce sufficiently large bite force at a gape width comparable to the leaf lamina thickness. For an ant of 3 mg, the strongest bites occur at a mandible gape of 0.1 mm, approximately half the median leaf thickness [79]. At 0.2 mm gape, the opening angle is only a few degrees larger and the force is almost identical ($\approx$ 99 %). If, however, this small ant had the same θ_{max} as the largest colony workers, the force at 0.2 mm would be 10 % less. We thus suggest that shifts in the optimal length such that the maximum bite force occurs at larger opening angles in small workers may represent an adaptive strategy to counter size-specific disadvantages when workers of different size forage on leaves with a similar thickness.

Positive allometry of bite force is common within, but rare across species

We discussed the mechanistic origin and ecological significance of the positive allometry of bite forces in *A. vollenweideri*. As a last step, we place our findings in a broader comparative and evolutionary context.

To this end, we compare both the scaling and magnitude of bite forces with two extensive datasets including close to 900 species, covering eight orders of magnitude in body mass and head volume [89, 90]. Regression analysis on $\log_{10}$-transformed bite force data for 203 amniote and two insect species against body mass [45, 46, 89], and for 139 amniote and 653 insect species against head volume [89, 90] suggests isometry of bite forces [$\text{mass}^{0.68}$, OLS 95 % CI: (0.65 | 0.72), $R^2 = 0.86$; head $\text{volume}^{0.68}$, OLS 95 % CI: (0.66 | 0.70), $R^2 = 0.87$, see Fig. 4]. The intercepts of the regression, which reflect mass- and head-volume specific bite forces (with mass in g, volume in mm^3, and force in N), in turn are -0.08 [mass across species: OLS 95 % CI: (-0.17 | 0.01)], 1.17 [mass within *A. vollenweideri*: OLS 95 % CI: (1.07 | 1.26), see Fig. 4C], -1.49 [volume across species: OLS 95 % CI: (-1.53 | -1.44)], and -1.29 [volume within *A. vollenweideri*: OLS 95 % CI: (-1.33 | -1.25)]. Leaf-cutter ants thus appear exceptional in at least two aspects: Their bite forces grow with strong positive allometry, and their weight-specific

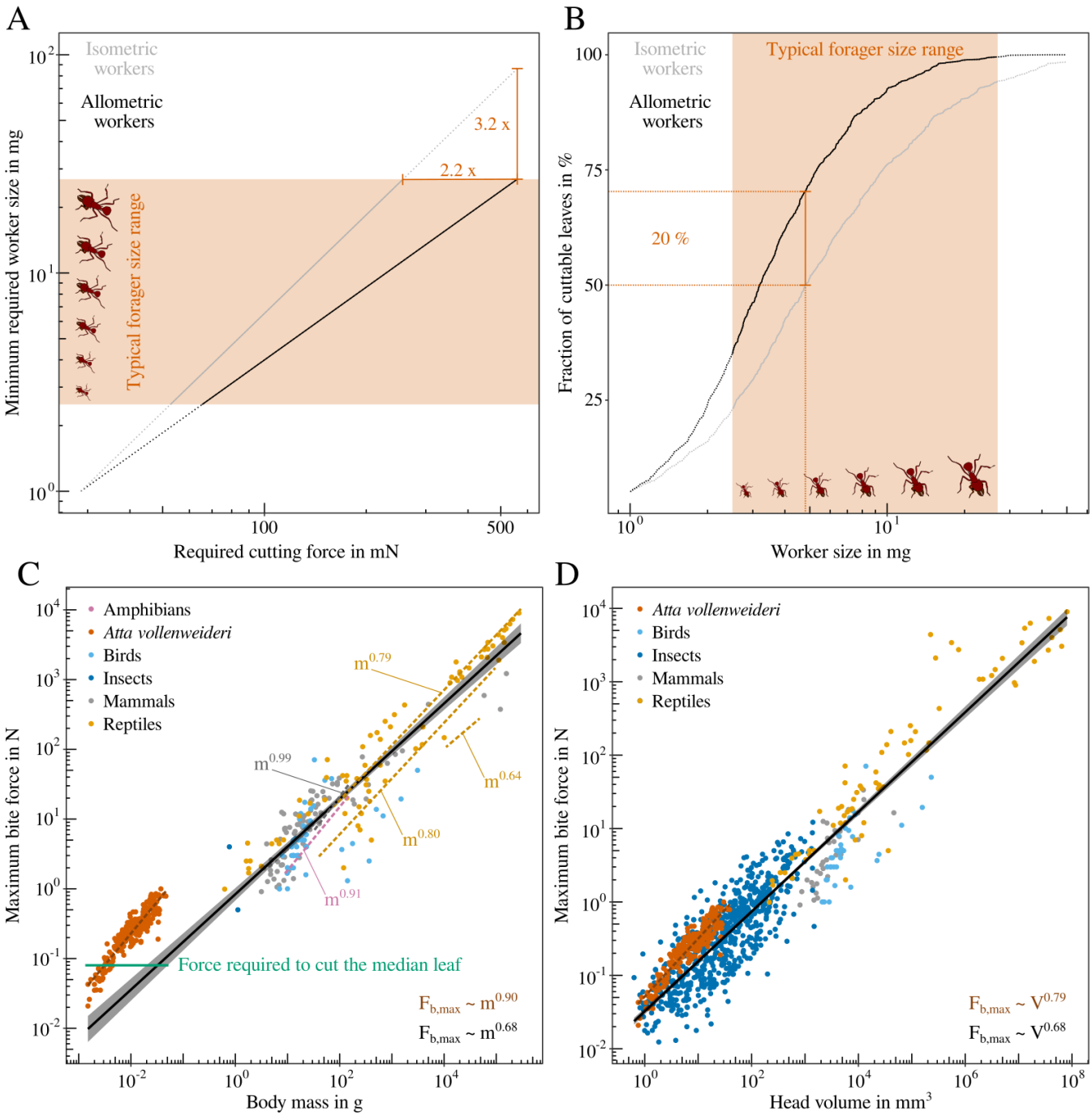

Figure 4 | (**A**) We consider possible benefits of the positive allometry of bite force by calculating the minimum worker size which can generate a given force, both for measured positively allometric and hypothetical isometric workers. An isometric worker needs to be about three times larger to produce the same bite force as the largest allometric forager; typical *Atta vollenweideri* foragers range between 2.5 to 26.9 mg [29]. (**B**) An allometric workforce increases the total fraction of cuttable leaves, estimated from measurements on 1000 tropical plant species [79], from around 94 % to almost 100 %. A medium-sized forager of about 5 mg can cut 70 % of leaves; its isometric counterpart only 50 %. The positive allometry of bite forces thus likely increases harvesting speed, and provides flexibility in task allocation, so enhancing colony fitness. (**C**) Positive allometry of bite force has been reported in intraspecific studies for several taxa [dashed lines, see 84–88, and Table 1]. Across distantly related species and a large size range, however, bite forces scale with isometry [black line, $\text{mass}^{0.68}$, OLS 95 % CI: (0.65 | 0.72), $R^2 = 0.86$]; each circle represents the average maximum bite force for a single species [extracted from 45, 46, 89]. *A. vollenweideri* ants generate exceptionally large weight-specific bite forces, comparable to those of amniotes 20 times heavier. (**D**) Relative to their head volume, however, their bite forces are comparable to those of other insects [extracted from 90], and amniotes [89], suggesting that leaf-cutter ants have a large weight-specific head volume. Across species, bite forces are isometric, head $\text{volume}^{0.68}$ [OLS 95 % CI: (0.66 | 0.70), $R^2 = 0.87$]. Within *A. vollenweideri*, however, bite force $\propto$ $\text{head volume}^{0.79}$ [OLS 95 % CI: (0.75 | 0.83), $R^2 = 0.86$], in excess of isometric predictions, due to a disproportionate increase in volume-specific physiological cross-sectional area of the mandible closer muscle [44].

bite forces are in substantial excess of that for the average amniote and insect, respectively [see also 47]; the largest ants produce maximum bite forces comparable to that of amniote species at least 20 times heavier (see Fig. 4C), and we have

Table 1 | Scaling of maximum bite forces for intraspecific (or intrageneric ‡) scaling studies across various taxa. The statistical models used to characterise the scaling relationships include Ordinary Least Squares (OLS) and Reduced Major Axis (RMA) regressions performed on $\log_{10}$-transformed data; in three studies, a non-linear RMA regression on untransformed data was used instead [86, 87, 91]. The relevant morphological variables are body mass (m), or one of several characteristic lengths, L: manus length (ML), snout vent length (SVL), carapace length (CL), and body length (BL). Where possible, we selected body mass as key variable to facilitate comparison with this study. A range of scaling coefficients is given when more than one species (or genus ‡), intraspecific morphotypes or sexual dimorphism were studied. Significant deviations from isometric scaling, *i* ($m^{0.67}$, L^2) are indicated with a *p* for positive allometry or *n* for negative allometry. We calculated a $\log_{10}$-transformed bite force quotient (BFQ) based on the reported mass range and regression coefficients [see 62, 92]. Because the BFQ is based on isometry, studies that reported allometric scaling are characterised by a range of BFQs. Where regression coefficients for body mass were missing, we calculated the range of BFQ based on the reported mass and bite force ranges (labelled with ∗). Bite forces that were not measured at the most distal tip of the jaws, or for which the bite position was not explicitly reported, are labelled with a †; these data are biased and thus need to be compared with care (see main text).

Taxon	Statistical model	Scaling	Allometry	$\log_{10}$(BFQ)	Source
Ants	OLS	$m^{0.90}$	*p*	2.50 - 2.85	this study
Ants	RMA	$m^{0.97}$	*p*	2.44 - 2.90	this study
Birds ‡	RMA	$m^{0.76-0.88}$	*i*	0.62 - 1.22 ∗	[93]
Crabs	not specified	$m^{0.82}$	*p*	2.66 - 2.94 †	[94]
Crabs ‡	OLS	$ML^{1.49}$	*n*	no mass reported	[95]
Crocodylians	OLS	$m^{0.79}$	*p*	1.92 - 2.36 †	[84]
Crocodylians	RMA	$m^{0.77-0.78}$	*p*	1.98 - 2.40 †	[96]
Frogs	RMA	$m^{0.91}$	*p*	1.59 - 1.88	[88]
Eels	not specified	$BL^{2.79-2.94}$	*p*	no mass reported †	[97]
Lizards ‡	RMA	$SVL^{3.83-4.60}$	*p*	1.27 - 2.34 ∗ †	[98]
Lizards	RMA	$SVL^{2.65-3.37}$	*p*	2.10 - 2.67 ∗ †	[99]
Lizards	OLS	$m^{0.57-0.73}$	*n*, *p*	2.02 - 2.36 ∗	[100]
Piranhas	OLS	$BL^{2.30}$	*p*	2.37 - 2.47 ∗	[101]
Ratfish	OLS	$BL^{2.34}$	*i*	2.07 ∗	[102]
Rodents	RMA	$m^{0.89-0.99}$	*p*	1.83 - 2.04	[85]
Rodents	RMA	$m^{1.11}$	*p*	1.91 - 2.06 ∗	[103]
Rodents	non-linear RMA	$m^{0.93-1.01}$	*p*	1.78 - 2.07	[91]
Rodents	OLS	$m^{0.83}$	*p*	1.78 - 2.06 ∗	[104]
Snakes	OLS	$m^{0.28}$	*n*	0.71 - 1.14 †	[105]
Turtles	RMA	$CL^{1.73-2.23}$	*n*, *i*	1.52 - 2.53 ∗ †	[99]
Turtles	RMA	$m^{0.98}$	*p*	1.90 - 2.48 †	[106]
Turtles	non-linear RMA	$m^{0.80}$	*p*	1.40 - 1.85	[86]
Turtles	non-linear RMA	$m^{0.64}$	*i*	1.33	[87]

argued above that such a remarkable magnitude of bite forces probably arises from the ecological need to cut tough plant matter. Notably, both the magnitude and the scaling of the bite force of leaf-cutter ants are less remarkable relative to head volume [$V^{0.79}$, OLS 95 % CI: (0.75 | 0.83), R^2 = 0.86, see Fig. 4D]. This discrepancy reflects the fact that a large share of the positive allometry of bite forces in leaf-cutter ants is achieved by a positive allometry of head volume [see 44], and that leaf-cutter ants, and perhaps insects in general, have relatively larger heads than vertebrates; indeed, the weight-specific head volume for *A. vollenweideri* is $671 \pm 74\,mm^3/g$ compared to $209 \pm 134\,mm^3/g$ for amniotes [see Fig. 4 and 89].

In the above argument, we have conflated evolutionary allometry involving different species, with static allometry involving individuals of the same species at identical ontogenetic stage [107]. In order to analyse if the static positive allometry of bite forces in leaf-cutter ants is indeed exceptional, and to facilitate a more appropriate comparison of the magnitude of bite forces, we collated results from 22 intraspecific and intrageneric scaling studies on bite force across twelve taxonomic groups (including this study, see Table 1. We note that the majority of intraspecific scaling studies report ontogenetic instead of static scaling coefficients). For each study, we then calculated a $\log_{10}$-transformed 'bite force quotient', $\log_{10}(\text{BFQ}) = \log_{10}(\text{bite force}/\text{body mass}^{2/3})$ in $N/kg^{2/3}$ [62, 92] as a measure for weight-specific bite performance. Leaf-cutter ants have

the highest $\log_{10}$(BFQ) apart from coconut crabs, for which bite force were measured at a favourable mechanical advantage [94, in contrast, we report bite forces for the maximum outlever and thus small mechanical advantage].

We conclude that leaf-cutter ants are highly specialised to produce large bite forces: (i) they have large heads relative to their body mass compared to vertebrates; (ii) the volume occupation of mandible closer muscle in these heads and (iii) the geometry of the bite apparatus are close to putative theoretical optima [44, 47]; and (iv), the estimated maximum stress of the mandible closer muscle is among the highest ever measured [47].

In sharp contrast to the magnitude of bite force, the positive static allometry appears to be less remarkable: around 70 % of available intraspecific studies reported significant positive allometry of bite forces, if often less pronounced [including one study that also reported negative allometry for other phenotypes of the same species, 100]). Remarkably, and with the notable exception of bats and finches [89, 108–111], bite force studies involving different genera typically report isometric scaling [89, 112, 113, and see meta-analysis above], or even modest negative allometry [85, 103, 114–117]. There thus appears to be a systematic difference between ontogenetic, static and evolutionary scaling of bite forces. To visualise this contrasting tendency, we superimpose a small selection of scaling relationships on the overall evolutionary slope (dashed lines in Fig. 4C). The ontogenetic, static and evolutionary allometry of bite forces appears as a weak instance of Simpson's paradox, where the slope of a regression line across many data points is substantially different from the slope obtained for subsets of the data – a result which appears to be common in biomechanical scaling studies [118–120]. Positive allometry of bite forces is likely associated with direct ecological advantages, related for example to the quantity and quality of accessible food sources [e. g. 84, 99, this study]. However, increased evolutionary rates of adaptive change in bite forces, required to drive departures from isometry, appear to be the exception rather than the norm, at least across amniotes [89].

Four factors may contribute to this seeming discrepancy: First, intraspecific and intrageneric studies on bite performance may be biased toward taxa which may be reasonably expected to face strong ecological or behavioural demands on their bite forces, so increasing the probability of departures from isometry [also see 121]. Second, strong positive allometry across many decades of mass is challenging if not impossible to achieve without fundamental 're-design' [122]; as illustrative example, a hypothetical leaf-cutter ant with a body mass of 3 g would have a closer muscle with a volume that exceeds that of its head capsule. Third, in particular 'static' scaling studies may often be limited by comparatively narrow size ranges [e. g. 117, 123], which increases the influence of biological variation and thus decreases the accuracy of the estimated allometric slope. Fourth, few of the available scaling studies accounted for potential size-specific biases in bite force measurements (see methods), and may thus report under- or overestimates of the allometric slope. Ultimately, the differences between ontogenetic, static and evolutionary allometry of bite forces reflect species-specific needs, coupled with complex developmental, evolutionary and ecological constraints [e.g. 58, 107, 121, 122, 124–129]. Untangling the influence of these different factors constitutes an exciting avenue for comparative and evolutionary work across disparate taxa, and a large range of body sizes.

Conclusion and outlook

Bite forces in leaf-cutter ants scale with strong positive allometry, driven and accurately predicted by morphological and physiological adaptations of the bite apparatus. The positive allometry enables the colony to access an increased number of plant species, and is thus ecologically meaningful. Our study adds strong quantitative evidence in support of the hypothesis that size-polymorphism and the associated variation in shape broadens a colony's access to food plants [2, 5, 82, 130, 131]. However, we acknowledge that the exact relationship between worker size, food plants and cutting behaviour is complex, and is influenced by nest distance [13], mandibular wear [38], and stridulation of the ant gaster, which can reduce force fluctuations during cutting [37, 132]. To fully integrate the mechanical results of this study with foraging behaviour, direct measurements of cutting forces with differently-sized mandibles as well as behavioural assays with materials of varying mechanical properties are needed; both are currently under way in our laboratory. We hope that such work will increase our understanding of the complex interactions between polymorphism, bite force allometry and foraging ecology in leaf-cutter ants.

Acknowledgments

We thank Peter Rühr and Alexander Blanke for their support on the validation of our bite force set-up, Daniela Römer for her generous support during the time of experiments, and Yusuke Onoda for sharing the leaf data. This study is part of a project that has received funding from the European Research Council (ERC) under the European Union's Horizon 2020 research and innovation programme (Grant agreement No. 851705), a European Collaborations Grant by Imperial College (both to DL), and a Company of Biologists travel grant to FP.

References

[1] Mueller UG, Schultz TR, Currie CR, Adams RM, Malloch D. 2001 The origin of the Attine ant-fungus mutualism. *The Quarterly Review of Biology* **76**: 169-197.

[2] Hölldobler B, Wilson EO. 2010 The leafcutter ants: civilization by instinct. W. W. Norton & Company, New York City, NY, USA.

[3] Fowler HG, Pagani MI, Da Silva OA, Forti LC, Vasconelos DL. 1989 A pest is a pest is a pest? the dilemma of neotropical leaf-cutting ants keystone taxa of natural ecosystems. *Enviromental Management* **13**: 671-675.

[4] Costa AN, Vasconcelos HL, Vieira-Neto EH, Bruna EM. 2008 Do herbivores exert top-down effects in neotropical savannas? estimates of biomass consumption by leaf-cutter ants. *Journal of vegetation science* **19**: 849–854.

[5] Wilson EO. 1980 Caste and division of labor in leaf-cutter ants (Hymenoptera: Formicidae: *Atta*): I. the overall pattern in *A. Sextens*. *Behavioral Ecology and Sociobiology* **7**: 143-156.

[6] Wirth R, Herz H, Ryel RJ, Beyschlag W, Hölldobler B. 2003 Herbivory of Leaf-Cutting Ants: A Case Study on *Atta colombica* in the Tropical Rainforest of Panama. Berlin, Heidelberg, New York: Springer Science & Business Media.

[7] Pielström S, Roces F. 2013 Sequential soil transport and its influence on the spatial organisation of collective digging in leaf-cutting ants. *Public Library of Science One* **8**: e57040.

[8] Wilson EO. 1980 Caste and division of labor in leaf-cutter ants (Hymenoptera: Formicidae: *Atta*): II. the ergonomic optimization of leaf cutting. *Behavioral Ecology and Sociobiology* **7**: 157-165.

[9] Wilson EO. 1983 Caste and division of labor in leaf-cutter ants (Hymenoptera: Formicidae: *Atta*): III. ergonomic resiliency in foraging by *A. cephalotes*. *Behavioral Ecology and Sociobiology* **14**: 47-54.

[10] Wilson EO. 1983 Caste and division of labor in leaf-cutter ants (Hymenoptera: Formicidae: *Atta*): IV. colony ontogeny of *A. cephalotes*. *Behavioral Ecology and Sociobiology* **14**: 55-60.

[11] Rudolph SG, Loudon C. 1986 Load size selection by foraging leaf-cutter ants (*Atta cephalotes*). *Ecological Entomology* **11**: 401-410.

[12] Wetterer JK. 1990 Load-size determination in the leaf-cutter ant, *Atta cephalotes*. *Behavioural Ecology* **1**: 95-101.

[13] Roces F. 1990 Leaf-cutting ants cut fragment sizes in relation to the distance from the nest. *Animal Behaviour* **40**: 1181-1183.

[14] Roces F, Núñez JA. 1993 Information about food quality influences load-size selection in recruited leaf-cutting ants. *Animal Behaviour* **45**: 135-143.

[15] Roces F, Hölldobler B. 1994 Leaf density and a trade-off between load-size selection and recruitment behaviour in the ant *Atta cephalotes*. *Oecologia* **97**: 1-8.

[16] Wetterer JK. 1994 Forager polymorphism, size-matching, and load delivery in the leaf-cutting ant, *Atta cephalotes*. *Ecological Entomology* **19**: 57-64.

[17] Wetterer JK. 1994 Ontogenetic changes in forager polymorphism and foraging ecology in the leaf-cutting ant *Atta cephalotes*. *Oecologia* **98**: 235-238.

[18] Wetterer JK. 1995 Forager polymorphism and foraging ecology in the leaf-cutting ant, *Atta colombica*. *Psyche* **102**: 131-145.

[19] Wetterer JK. 1995 Forager size and ecology of *Acromyrmex coronatus* and other leaf-cutting ants in costa rica. *Oecologia* **104**: 409-415.

[20] Burd M. 1995 Variable load size-ant size matching in leaf-cutting ants, *Atta colombica* (Hymenoptera: Formicidae). *Journal of Insect Behavior* **8**: 715-722.

[21] Roces F, Hölldobler B. 1996 Use of stridulation in foraging leaf-cutting ants: mechanical support during cutting or short-range recruitment signal? *Behavioral Ecology and Sociobiology* .

[22] Burd M. 1996 Foraging performance by *Atta colombica*, a leaf-cutter ant. *The American Naturlist* **148**: 597-612.

[23] Burd M. 2000 Body size effects on locomotion and load carriage in the highly polymorphic leaf-cutting ants *Atta colombica* and *Atta cephalotes*. *Behavioral Ecology* **11**: 125-131.

[24] Burd M. 2000 Foraging behaviour of *Atta cephalotes* (leaf-cutting ants): an examination of two predictions for load selection. *Animal Behaviour* **60**: 781-788.

[25] Burd M. 2001 Leaf tissue transport as a function of loading ratio in the leaf-cutting ant *Atta cephalotes*. *Ecological Entomology* **26**: 551-556.

[26] Farji-Brener AG. 2001 Why are leaf-cutting ants more common in secondary forest than in old-growth tropical forests? an evaluation of the palatable forage hypothesis. *Oikos* **92**: 169-177.

[27] Röschard J, Roces F. 2002 The effect of load length, width and mass on transport rate in the grass-cutting ant *Atta vollenweideri*. *Oecologia* **131**: 319-324.

[28] Farji-Brener AG, Sasal Y. 2003 Is dump material an effective small-scale deterrent to herbivory by leaf-cutting ants? *Ecoscience* **10**: 151–154.

[29] Röschard J, Roces F. 2003 Fragment-size determination and size-matching in the grass-cutting ant *Atta vollenweideri* depend on the distance from the nest. *Journal of Tropical Ecology* **19**: 647-653.

[30] Burd M, Howard JJ. 2005 Central-place foraging continues beyond the nest entrance: the underground performance of leaf-cutting ants. *Animal Behaviour* **70**: 737-744.

[31] Dussutour A, Deneubourg JL, Beshers S, Fourcassié V. 2008 Individual and collective problem-solving in a foraging context in the leaf-cutting ant *Atta colombica*. *Animal cognition* **12**: 21-30.

[32] Moll K, Roces F, Federle W. 2010 Foraging grass-cutting ants (*Atta vollenweideri*) maintain stability by balancing their loads with controlled head movements. *Journal of Comparative Physiology A* **196**: 471-480.

[33] Röschard J, Roces F. 2011 Sequential load transport in grass-cutting ants (*Atta vollenweideri*): maximization of plant delivery rate or improved information transfer? *Psyche* **2011**: ID 643127.

[34] Moll K, Roces F, Federle W. 2013 How load-carrying ants avoid falling over: mechanical stability during foraging in *Atta vollenweideri* grass-cutting ants. *Public Library of Science One* **8**: e52816.

[35] Roces F, Lighton JR. 1995 Larger bites of leaf-cutting ants. *Nature* **373**: 392.

[36] Roces F. 2002 Individual complexity and self-organization in foraging by leaf-cutting ants. *The Biological Bulletin* **202**: 306-312.

[37] Tautz J, Roces F, Hölldobler B. 1995 Use of a sound-based vibratome by leaf-cutting ants. *Science* **267**: 84.

[38] Schofield RM, Emmett KD, Niedbala JC, Nesson M. 2011 Leaf-cutter ants with worn mandibles cut half as fast, spend twice the energy, and tend to carry instead of cut. *Behavioral Ecology and Sociobiology* **65**: 969-982.

[39] Schofield RM, Choi S, Coon JJ, Goggans MS, Kreisman TF, Silver DM, Nesson MH. 2016 Is fracture a bigger problem for smaller animals? force and fracture scaling for a simple model of cutting, puncture and crushing. *Interface Focus* **6**.

[40] Cherrett JM. 1972 Some factors involved in the selection of vegetable substrate by *Atta cephalotes* (l.) (hymenoptera: Formicidae) in tropical rain forest. *Journal of Animal Ecology* **41**: 647-660.

[41] Nichols-Orians CM, Schultz JC. 1989 Leaf toughness affects leaf harvesting by the leaf cutter ant, *Atta cephalotes* (l.) (Hymenoptera: Formicidae). *Biotropica* **21**: 80-83.

[42] Nichols-Orians CM, Schultz JC. 1990 Interactions among leaf toughness, chemistry, and harvesting by attine ants. *Ecological Entomology* **15**: 311-320.

[43] Wetterer JK. 1991 Allometry and geometry of leaf-cutting in *Atta cephalotes*. *Behavioral Ecology and Sociobiology* **29**: 347-351.

[44] Püffel F, Pouget A, Liu X, Zuber M, van de Kamp T, Roces F, Labonte D. 2021 Morphological determinants of bite force capacity in insects: a biomechanical analysis of polymorphic leaf-cutter ants. *Journal of the Royal Society Interface* **18**: 20210424.

[45] Goyens J, Dircks J, Dierick M, Van Hoorebeke L, Aerts P. 2014 Biomechanical determinants of bite force dimorphism in *Cyclommatus metallifer* stag beetles. *Journal of Experimental Biology* **217**: 1065-1071.

[46] Weihmann T, Reinhardt L, Weißing K, Siebert T, Wipfler B. 2015 Fast and powerful: Biomechanics and bite forces of the mandibles in the american cockroach *Periplaneta americana*. *Public Library of Science One* **10**: e0141226.

[47] Püffel F, Johnston RE, Labonte D. 2022 A general biomechanical model for the relation between bite force and mandibular opening angle in arthropods. *bioRxiv* .

[48] Van Rossum G, Drake FL. 2009 Python 3 Reference Manual. Scotts Valley, CA: CreateSpace.

[49] Haykin S. 2001 Communication Systems. John Wiley & Sons, Inc., 4 edition.

[50] Herrel A, Spithoven L, Van Damme R, De Vree F. 1999 Sexual dimorphism of head size in gallotia galloti: testing the niche divergence hypothesis by functional analyses. *Functional Ecology* **13**: 289–297.

[51] Rühr PT, Blanke A. 2022 forcex and forcer: a mobile setup and r package to measure and analyse a wide range of animal closing forces. *Methods in Ecology and Evolution* : 1–11.

[52] Weihmann T, Kleinteich T, Gorb SN, Wipfler B. 2015 Functional morphology of the mandibular apparatus in the cockroach *Periplaneta americana* (blattodea: Blattidae) – a model species for omnivore insects. *Arthropod Systematics & Phylogeny* **73**: 477-488.

[53] Lappin AK, Jones ME. 2014 Reliable quantification of bite-force performance requires use of appropriate biting substrate and standardization of bite out-lever. *Journal of Experimental Biology* **217**: 4303–4312.

[54] Gordon A, Huxley AF, Julian F. 1966 The variation in isometric tension with sarcomere length in vertebrate muscle fibres. *The Journal of physiology* **184**: 170–192.

[55] Josephson RK. 1975 Extensive and intensive factors determining the performance of striated muscle. *Journal of Experimental Zoology* **194**: 135–153.

[56] Otten E. 1987 Optimal design of vertebrate and insect sarcomeres. *Journal of Morphology* **191**: 49–62.

[57] R Core Team. 2021 R: A Language and Environment for Statistical Computing. R Foundation for Statistical Computing, Vienna, Austria. URL `https://www.R-project.org/`.

[58] LaBarbera M. 1989 Analyzing body size as a factor in ecology and evolution. *Annual review of ecology and systematics* : 97–117.

[59] Clissold F. 2007 The biomechanics of chewing and plant fracture: Mechanisms and implications. *Advances in Insect Physiology* **34**.

[60] Erickson GM, Kirk SDV, Su J, Levenston ME, Caler WE, Carter DR. 1996 Bite-force estimation for tyrannosaurus rex from tooth-marked bones. *Nature* **382**: 706–708.

[61] Huber DR, Weggelaar CL, Motta PJ. 2006 Scaling of bite force in the blacktip shark *Carcharhinus limbatus*. *Zoology* **109**: 109–119.

[62] Heethoff M, Norton RA. 2009 A new use for synchrotron x-ray microtomography: three-dimensional biomechanical modeling of chelicerate mouthparts and calculation of theoretical bite forces. *Invertebrate Biology* **128**: 332–339.

[63] Habegger ML, Motta PJ, Huber DR, Dean MN. 2012 Feeding biomechanics and theoretical calculations of bite force in bull sharks (*Carcharhinus leucas*) during ontogeny. *Zoology* **115**: 354–364.

[64] Taylor GM. 2000 Maximum force production: why are crabs so strong? *Proceedings of the Royal Society of London. Series B: Biological Sciences* **267**: 1475–1480.

[65] Guschlbauer C, Scharstein H, Büschges A. 2007 The extensor tibiae muscle of the stick insect: biomechanical properties of an insect walking leg muscle. *Journal of Experimental Biology* **210**: 1092–1108.

[66] Anderson RA, McBrayer LD, Herrel A. 2008 Bite force in vertebrates: opportunities and caveats for use of a nonpareil whole-animal performance measure. *Biological Journal of the Linnean Society* **93**: 709–720.

[67] Dumont ER, Herrel A. 2003 The effects of gape angle and bite point on bite force in bats. *Journal of Experimental Biology* **206**: 2117–2123.

[68] Gidmark NJ, Konow N, LoPresti E, Brainerd EL. 2013 Bite force is limited by the force–length relationship of skeletal muscle in black carp, *Mylopharyngodon piceus*. *Biology Letters* **9**: 20121181.

[69] Santana SE. 2016 Quantifying the effect of gape and morphology on bite force: biomechanical modelling and *in vivo* measurements in bats. *Functional Ecology* **30**: 557–565.

[70] Kaczmarek EB, Gidmark NJ. 2020 The bite force–gape relationship as an avenue of biomechanical adaptation to trophic niche in two salmonid fishes. *Journal of Experimental Biology* **223**: jeb223180.

[71] Cherrett JM. 1968 The foraging behaviour of *Atta cephalotes* l. (Hymenoptera, Formicidae). *Journal of Animal Ecology* **37**: 387-403.

[72] Rockwood LL. 1976 Plant selection and foraging patterns in two species of leaf-cutting ants (*Atta*). *Ecology* **57**: 48-61.

[73] Shepherd JD. 1985 Adjusting foraging effort to resources in adjacent colonies of the leaf-cutter ant, *Atta colombica*. *Biotropica* **17**: 245-252.

[74] Waller D. 1982 Leaf-cutting ants and live oak: the role of leaf toughness in seasonal and intraspecific host choice. *Entomologia Experimentalis et Applicata* **32**: 146-150.

[75] Kamyab I, Chakrabati S, Williams JG. 1998 Cutting cheese with wire. *Journal of Materials Science* **33**: 2763-2770.

[76] Williams JG, Patel Y. 2016 Fundamentals of cutting. *Interface Focus* **6**: 20150108.

[77] Zhang B, Shiang CS, Yang SJ, Hutchens SB. 2019 Y-shaped cutting for the systematic characterization of cutting and tearing. *Experimental Mechanics* **59**: 517–529.

[78] Darvell B, Lee P, Yuen T, Lucas P. 1996 A portable fracture toughness tester for biological materials. *Measurement Science and Technology* **7**: 954.

[79] Onoda Y, Westoby M, Adler PB, Choong AMF, Clissold FJ, Cornelissen JHC, Díaz S, Dominy NJ, Elgart A, Enrico L, Fine PVA, Howard JJ, Jalili A, Kitajima K, Kurokawa H, McArthur C, Lucas PW, Markesteijn L, Pérez-Harguindeguy N, Poorter L, Richards L, Santiago LS, Sosinski Jr EE, Van Bael SA, Warton DI, Wright IJ, Joseph Wright S, Yamashita N. 2011 Global patterns of leaf mechanical properties. *Ecology Letters* **14**: 301-312.

[80] Fowler H, Forti L, Pereira-da Silva V, Saes N. 1986 Economics of grass-cutting ants. In: Fire ants and leaf-cutting ants, CRC Press. pp. 18–35.

[81] Wilson EO. 1953 The origin and evolution of polymorphism in ants. *The Quartely Review of Biology* **28**: 136-156.

[82] Wetterer JK. 1999 The ecology and evolution of worker size-distribution in leaf-cutting ants (hymenoptera: Formicidae). *Sociobiology* **34**: 119-144.

[83] Evison SE, Ratnieks FL. 2007 New role for majors in *Atta* leaf-cutter ants. *Ecological Entomology* **32**: 451–454.

[84] Erickson GM, Lappin AK, Vliet KA. 2003 The ontogeny of bite-force performance in american alligator (*Alligator mississippiensis*). *Journal of Zoology* **260**: 317–327.

[85] Becerra F, Echeverría A, Vassallo AI, Casinos A. 2011 Bite force and jaw biomechanics in the subterranean rodent talas tuco-tuco (*Ctenomys talarum*)(caviomorpha: Octodontoidea). *Canadian Journal of Zoology* **89**: 334–342.

[86] Marshall CD, Guzman A, Narazaki T, Sato K, Kane EA, Sterba-Boatwright BD. 2012 The ontogenetic scaling of bite force and head size in loggerhead sea turtles (*Caretta caretta*): implications for durophagy in neritic, benthic habitats. *Journal of Experimental Biology* **215**: 4166–4174.

[87] Marshall CD, Wang J, Rocha-Olivares A, Godinez-Reyes C, Fisler S, Narazaki T, Sato K, Sterba-Boatwright BD. 2014 Scaling of bite performance with head and carapace morphometrics in green turtles (chelonia mydas). *Journal of Experimental Marine Biology and Ecology* **451**: 91–97.

[88] Lappin AK, Wilcox SC, Moriarty DJ, Stoeppler SA, Evans SE, Jones ME. 2017 Bite force in the horned frog (*Ceratophrys cranwelli*) with implications for extinct giant frogs. *Scientific reports* **7**: 1–10.

[89] Sakamoto M, Ruta M, Venditti C. 2019 Extreme and rapid bursts of functional adaptations shape bite force in amniotes. *Proceedings of the Royal Society B* **286**: 20181932.

[90] Rühr PT, Edel C, Frenzel M, Blanke A. 2022 A bite force database of 654 insect species. *bioRxiv* .

[91] Vassallo AI, Becerra F, Echeverría AI, Casinos A. 2016 Ontogenetic integration between force production and force reception: a case study in ctenomys (rodentia: Caviomorpha). *Acta Zoologica* **97**: 232–240.

[92] van der Meijden A, Langer F, Boistel R, Vagovic P, Heethoff M. 2012 Functional morphology and bite performance of raptorial chelicerae of camel spiders (solifugae). *Journal of experimental biology* **215**: 3411–3418.

[93] Sustaita D, Hertel F. 2010 In vivo bite and grip forces, morphology and prey-killing behavior of north american accipiters (accipitridae) and falcons (falconidae). *Journal of Experimental Biology* **213**: 2617–2628.

[94] Oka Si, Tomita T, Miyamoto K. 2016 A mighty claw: pinching force of the coconut crab, the largest terrestrial crustacean. *Public Library of Science One* **11**: e0166108.

[95] Palmer AR, Taylor GM, Barton A. 1999 Cuticle strength and the size-dependence of safety factors in *Cancer* crab claws. *The Biological Bulletin* **196**: 281–294.

[96] Erickson G, Gignac P, Lappin A, Vliet K, Brueggen J, Webb G. 2014 A comparative analysis of ontogenetic bite-force scaling among crocodylia. *Journal of Zoology* **292**: 48–55.

[97] De Meyer J, Herrel A, Belpaire C, Goemans G, Ide C, De Kegel B, Christiaens J, Adriaens D. 2018 Broader head, stronger bite: *In vivo* bite forces in european eel *Anguilla anguilla*. *Journal of Fish Biology* **92**: 268–273.

[98] Meyers JJ, Herrel A, Birch J. 2002 Scaling of morphology, bite force and feeding kinematics in an iguanian and a scleroglossan lizard. *Topics in Functional and Ecological Vertebrate Morphology* : 47 – 62.

[99] Herrel A, O'Reilly JC. 2006 Ontogenetic scaling of bite force in lizards and turtles. *Physiological and Biochemical Zoology* **79**: 31–42.

[100] Jones ME, Pistevos JC, Cooper N, Lappin AK, Georges A, Hutchinson MN, Holleley CE. 2020 Reproductive phenotype predicts adult bite-force performance in sex-reversed dragons (*Pogona vitticeps*). *Journal of Experimental Zoology Part A: Ecological and Integrative Physiology* **333**: 252–263.

[101] Grubich JR, Huskey S, Crofts S, Orti G, Porto J. 2012 Mega-bites: extreme jaw forces of living and extinct piranhas (serrasalmidae). *Scientific Reports* **2**: 1–9.

[102] Huber DR, Dean MN, Summers AP. 2008 Hard prey, soft jaws and the ontogeny of feeding mechanics in the spotted ratfish *Hydrolagus colliei*. *Journal of the Royal Society Interface* **5**: 941–953.

[103] Becerra F, Casinos A, Vassallo AI. 2013 Biting performance and skull biomechanics of a chisel tooth digging rodent (*Ctenomys tuconax*; caviomorpha; octodontoidea). *Journal of Experimental Zoology Part A: Ecological Genetics and Physiology* **319**: 74–85.

[104] Ginot S, Hautier L, Agret S, Claude J. 2020 Decoupled ontogeny of *in vivo* bite force and mandible morphology reveals effects of weaning and sexual maturation in mice. *Biological Journal of the Linnean Society* **129**: 558–569.

[105] Penning DA. 2017 The scaling of bite force and constriction pressure in kingsnakes (*Lampropeltis getula*): proximate determinants and correlated performance. *Integrative Zoology* **12**: 121–131.

[106] Pfaller J, Herrera N, Gignac P, Erickson G. 2010 Ontogenetic scaling of cranial morphology and bite-force generation in the loggerhead musk turtle. *Journal of Zoology* **280**: 280–289.

[107] Pélabon C, Bolstad GH, Egset CK, Cheverud JM, Pavlicev M, Rosenqvist G. 2013 On the relationship between ontogenetic and static allometry. *The American Naturalist* **181**: 195–212.

[108] Aguirre LF, Herrel A, Van Damme R, Matthysen E. 2002 Ecomorphological analysis of trophic niche partitioning in a tropical savannah bat community. *Proceedings of the Royal Society of London. Series B: Biological Sciences* **269**: 1271–1278.

[109] van der Meij M, Bout R. 2004 Scaling of jaw muscle size and maximal bite force in finches. *Journal of Experimental Biology* **207**: 2745–2753.

[110] Herrel A, Podos J, Huber S, Hendry A. 2005 Evolution of bite force in darwin's finches: a key role for head width. *Journal of Evolutionary Biology* **18**: 669–675.

[111] Senawi J, Schmieder D, Siemers B, Kingston T. 2015 Beyond size - morphological predictors of bite force in a diverse insectivorous bat assemblage from malaysia. *Functional Ecology* **29**: 1411–1420.

[112] Huber DR, Eason TG, Hueter RE, Motta PJ. 2005 Analysis of the bite force and mechanical design of the feeding mechanism of the durophagous horn shark *Heterodontus francisci*. *Journal of Experimental Biology* **208**: 3553–3571.

[113] Deeming D. 2022 Inter-relationships among body mass, body dimensions, jaw musculature and bite force in reptiles. *Journal of Zoology* : 1–11.

[114] Claussen DL, Gerald GW, Kotcher JE, Miskell CA. 2008 Pinching forces in crayfish and fiddler crabs, and comparisons with the closing forces of other animals. *Journal of Comparative Physiology B* **178**: 333–342.

[115] Huber DR, Claes JM, Mallefet J, Herrel A. 2009 Is extreme bite performance associated with extreme morphologies in sharks? *Physiological and Biochemical Zoology* **82**: 20–28.

[116] Van Daele P, Herrel A, Adriaens D. 2009 Biting performance in teeth-digging african mole-rats (*Fukomys*, bathyergidae, rodentia). *Physiological and Biochemical Zoology* **82**: 40–50.

[117] Hite NJ, Germain C, Cain BW, Sheldon M, Perala SSN, Sarko DK. 2019 The better to eat you with: bite force in the naked mole-rat (*Heterocephalus glaber*) is stronger than predicted based on body size. *Frontiers in Integrative Neuroscience* **13**: 70.

[118] Schmidt-Nielsen K, Knut SN. 1984 Scaling: why is animal size so important? Cambridge university press.

[119] Peattie A, Full R. 2007 Phylogenetic analysis of the scaling of wet and dry biological fibrillar adhesives. *Proceedings of the National Academy of Sciences* **104**: 18595–18600.

[120] Labonte D, Clemente CJ, Dittrich A, Kuo CY, Crosby AJ, Irschick DJ, Federle W. 2016 Extreme positive allometry of animal adhesive pads and the size limits of adhesion-based climbing. *Proceedings of the National Academy of Sciences* **113**: 1297–1302.

[121] Bonduriansky R. 2007 Sexual selection and allometry: a critical reappraisal of the evidence and ideas. *Evolution: International Journal of Organic Evolution* **61**: 838–849.

[122] Gould SJ. 1966 Allometry and size in ontogeny and phylogeny. *Biological reviews* **41**: 587–638.

[123] Herrel A, Damme RV, Vanhooydonck B, Vree FD. 2001 The implications of bite performance for diet in two species of lacertid lizards. *Canadian Journal of Zoology* **79**: 662–670.

[124] Smith RJ. 1984 Allometric scaling in comparative biology: problems of concept and method. *American Journal of Physiology-Regulatory, Integrative and Comparative Physiology* **246**: 152–160.

[125] Egset CK, Hansen TF, Le Rouzic A, Bolstad GH, Rosenqvist G, Pelabon C. 2012 Artificial selection on allometry: change in elevation but not slope. *Journal of evolutionary biology* **25**: 938–948.

[126] Voje KL, Hansen TF. 2013 Evolution of static allometries: adaptive change in allometric slopes of eye span in stalk-eyed flies. *Evolution: International Journal of Organic Evolution* **67**: 453–467.

[127] Pélabon C, Firmat C, Bolstad GH, Voje KL, Houle D, Cassara J, Rouzic AL, Hansen TF. 2014 Evolution of morphological allometry. *Annals of the New York Academy of Sciences* **1320**: 58–75.

[128] Voje KL, Hansen TF, Egset CK, Bolstad GH, Pelabon C. 2014 Allometric constraints and the evolution of allometry. *Evolution* **68**: 866–885.

[129] Bolstad GH, Cassara JA, Márquez E, Hansen TF, van der Linde K, Houle D, Pélabon C. 2015 Complex constraints on allometry revealed by artificial selection on the wing of *Drosophila melanogaster*. *Proceedings of the National Academy of Sciences* **112**: 13284–13289.

[130] Waller D. 1989 Size-related foraging in the leaf-cutting ant *Atta texana* (buckley) (formicidae: Attini). *Functional Ecology* **3**: 461-468.

[131] Clark E. 2006 Dynamic matching of forager size to resources in the continuously polymorphic leaf-cutter ant, *Atta colombica* (hymenoptera, formicidae). *Ecological Entomology* **31**: 629-635.

[132] Roces F. 2022 Vibrational communication outside and inside the nest in leaf-cutting ants. In: Biotremology: Physiology, Ecology, and Evolution, Springer. pp. 411–435.

Supplementary Materials

Effects of bite plate deflection during biting

During bite force measurements, maximum forces of around $F = 1\,\mathrm{N}$ were applied onto the bite plates. We estimate the magnitude of plate deflection caused by these forces, δ_{max}, by invoking a result from simple beam theory: $\delta_{max} = FL/EHT^3$, where L is the protruding length of the bite plate (1 mm), H its height (6 mm), and T its thickness ($\approx 0.15\,\mathrm{mm}$). Using a typical Young's modulus for stainless steel ($E \approx 200\,\mathrm{GPa}$), the deflection is at most $\delta_{max} = 0.0002\,\mathrm{mm}$. We hence neglected any effects of plate deflection.

Force sensor circuit and user interface

A custom-built force set-up was developed to measure bite forces of ants and other small insects. The bite forces were measured using a capacitive force sensor, connected to a raspberry pi via I^2C board (see Fig. 5A). The pi is also connected to a stepper motor via driver board, to adjust the distance between two bite plates, a camera module to record the bite experiments simultaneously to the sensor readings, and a LCD touchscreen (see main text). A user interface, written in Python (v 3.5) enables the operator to calibrate the force sensor, start and stop the force and video recordings, set the current sensor reading to zero, display live outputs of force sensor and camera, save the measurements, and to adjust the plate distance.

Projection of the mandibular joint rotational axis

We determined the mandibular joint axis of rotation $\hat{\mathbf{R}}$ via kinematics analysis of the mandible motion [V Kang, F Püffel and D Labonte, in preparation]. We assumed that the relative orientation of $\hat{\mathbf{R}}$ to the head coordinate system of the scans, defined in [44], is size-invariant. However, the relative position of $\hat{R}$ with respect to the head coordinate system defined for biting ants, may differ, because it is difficult to find the same key locations for all bite force recordings. We thus defined a second coordinate system based on the coordinates of the mandible joint and the two distinct head spikes (see main text). To quantify the variation of $\hat{R}$ due to difference in spike location across sizes, $\hat{R}$ was projected from the scan coordinate system to the spike-based coordinate systems of all scans. The angular difference between the projections of $\hat{R}$ and their mean was small, $4 \pm 1^\circ$ with no significant size effect (Pearson's correlation coefficient: $r_{11} = 0.46$, $P = 0.12$). We hence selected the mean orientation of $\hat{R}$ with respect to the head spikes for all sizes for the bite video analysis (see main text).

Filament length

The length of the filaments L_{fil} connecting muscle fibres and apodeme determines the relationship between muscle fibre length and mandibular opening angle, as detailed in [47]. We estimated L_{fil} as the difference between the internal radius and apodeme radius, $L_{fil} = r_i - r_{apo}$. The internal radius represents the effective radius of attachment; the apodeme radius was defined as the equivalent radius of the apodeme cross-sectional area, assuming a circular shape, [see 44, for an exact definition].

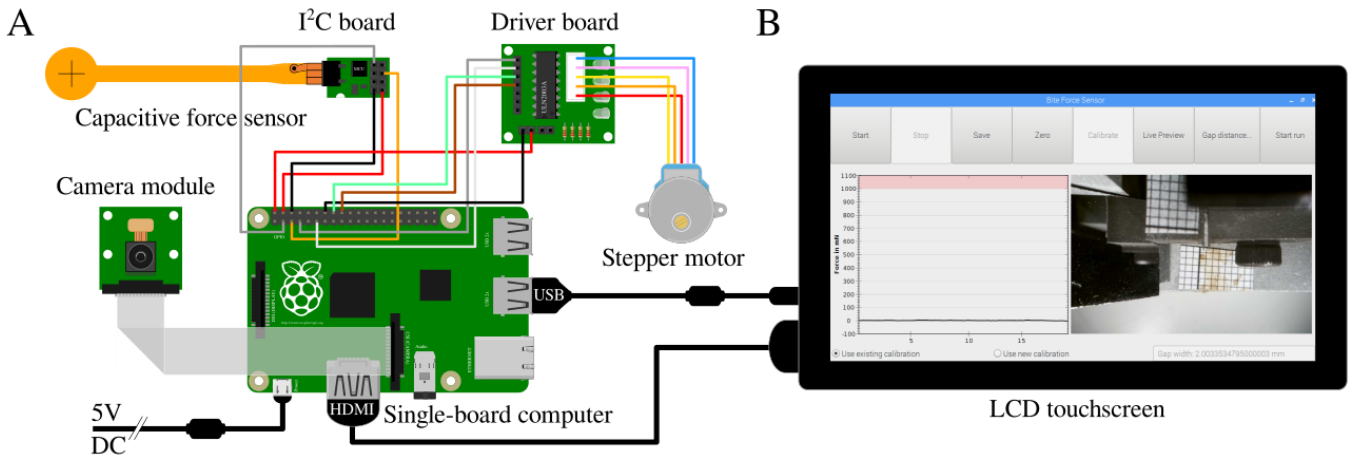

Figure 5 | (**A**) We developed a force set-up to accurately measure bite forces of small insect. Bite forces were measured by compressing a capacitive force sensor, sampled at 33 Hz (for more details, see main text). The sensor is connected to a raspberry pi via an I^2C board. The pi, powered at 5 V DC, is also connected to a stepper motor via driver board, a camera module, and a LCD touchscreen. (**B**) A user interface, written in Python (v 3.5), enables the experimenter to calibrate the force sensor, start and stop the force and video recordings, set current force readings to zero, show live readings of forces and camera output, save measurements, and move the stepper motor.

Table 2 | Results of reduced major axis regressions describing the relationship of bite force with body mass and head volume (labelled with $*$), respectively, on $\log_{10}$-transformed data. 95 % confidence intervals are provided in parentheses.

Description	Units	Elevation	Slope	R^2
Morphological prediction	mN, mg	1.41 (1.31, 1.51)	0.93 (0.84, 0.1.03)	0.98
Fully-corrected measurement	mN, mg	1.38 (1.34, 1.43)	0.97 (0.93, 1.02)	0.86
Angle-uncorrected measurement	mN, mg	1.12 (1.05, 1.19)	0.99 (0.93, 1.06)	0.74
Raw measurement	mN, mg	1.33 (1.27, 1.39)	0.91 (0.86, 0.97)	0.75
Fully-corrected measurement $*$	N, mm^3	-1.34 (-1.38, -1.30)	0.85 (0.81, 0.89)	0.86
Meta-analysis	N, g	-0.18 (-0.27, -0.09)	0.74 (0.70, 0.77)	0.86
Meta-analysis $*$	N, mm^3	-1.59 (-1.63, -1.54)	0.91 (0.86, 0.97)	0.87

Table 3 | Results of reduced major axis regressions describing the relationship of mandibular opening angle in degrees, (i) at which muscle fibre length is optimum, θ_{opt}, and (ii) at which bite forces are maximum, θ_{max}, with body mass in mg on $\log_{10}$-transformed data. 95 % confidence intervals are provided in parentheses.

Quantity	Elevation	Slope	R^2
θ_{opt}	1.89 (1.83, 1.95)	-0.13 (-0.19, -0.08)	0.56
θ_{max}	1.83 (1.79, 1.87)	-0.08 (-0.12, -0.05)	0.59